FACTA UNIVERSITATIS
Series: **Mechanical Engineering**
https://doi.org/10.22190/FUME210714068B

Original scientific paper

IMPROVING CORROSION RESISTANCE OF MAGNESIUM NANOCOMPOSITES BY USING ELECTROLESS NICKEL COATINGS

Sudip Banerjee[1], Pujan Sarkar[2], Prasanta Sahoo[1]

[1]Department of Mechanical Engineering, Jadavpur University, Kolkata, India
[2]Jaipaiguri Polytechnic Institute, Jalpaiguri, West Bengal, India

Abstract. *The present study aims at improving corrosion resistance of magnesium nanocomposites through autocatalytic Ni-P coating. Electroless Ni-P coatings with different concentration of sodium hypophosphite are deposited on 2% WC incorporated magnesium nanocomposites (AZ31-2WC) and the coated samples are further heat-treated. Basic characterizations and compositional analyses are done by using scanning electron microscope (SEM), energy dispersive x-ray analysis (EDAX), and X-ray diffraction analysis (XRD). Microhardness values of the developed materials are also evaluated. The attempt is made to improve corrosion resistance of AZ31-2WC by modifying surface roughness. Corrosion characteristics of Ni-P coated AZ31-2WC nanocomposites are examined by performing potentiodynamic polarization test and electrochemical impedance spectroscopy (EIS). Corrosion resistance improves with enhancement of surface quality. Corrosion resistance of AZ31-2WC nanocomposite also improves due to application of Ni-P coating. Finally, corrosion morphologies are scrutinized by SEM micrographs of corroded surface.*

Key Words: *Corrosion Resistance, Magnesium, Nanocomposite, Ni-P, Coating*

1. INTRODUCTION

Automobile industries are in search of lightweight materials due to the sky rocketing price of fuels and ever-stricter emission norms. In this regard, magnesium and magnesium-based composites have got attention of research fraternity, as they possess noticeable properties like high strength/weight ratio, superior hardness, high stiffness and good castability [1]. Accordingly, automotive sectors are trying to reinstate different ferrous components (transmission cases, steering shaft, power trains, housings, pistons

Received July 14, 2021 / Accepted November 14, 2021
Corresponding author: Prasanta Sahoo
Department of Mechanical Engineering, Jadavpur University, Kolkata-700032, India
E-mail: psjume@gmail.com; prasanta.sahoo@jadavpuruniversity.in

etc.) with magnesium based lightweight materials [2]. Literature reveals that incorporation of ceramic-based reinforcements can provide enhanced mechanical and tribological properties. However, particle size (micro/nano) of reinforcement phases also has noteworthy importance along with types of reinforcements while trying to attain enhanced properties. Usually, a higher amount of reinforcement is needed for micron size reinforcement compared to nano-sized reinforcements. Researchers reported that nearly two percentage of nano-sized reinforcement is adequate to achieve desired properties [3]. In this context, the researchers have fortified nanoparticles like SiC, TiC, TiB_2, WC, ZrO_2, Al_2O_3, BN, ZnO, graphite in magnesium matrix [3-9]. It was observed that mechanical and tribological properties are enhanced due to incorporation of those nanoparticles having varying weight percentage. Consequently, Banerjee et al. [9-12] incorporated different wt. % of WC nanoparticles in AZ31 matrix through ultrasonic vibration associated stir casting method and evaluated mechanical as well as tribological behavior at different experimental conditions. Microhardness, nanohardness and elastic modulus of 2% WC incorporated magnesium nanocomposites (AZ31-2WC) were found to be enhanced by 53%, 122% and 170%, respectively, compared to AZ31 alloy. Even tribological behavior (friction and wear) of Az31-2WC nanocomposite possessed significant improvement comparing to AZ31 alloy in dry sliding, under elevated temperature conditions and also in abrasive conditions for different parametric variations of sliding speed, load, and sliding distance. Thus, overall AZ31-2WC nanocomposite is found to possess excellent mechanical and tribological properties. However, the chemical affinity of magnesium-based materials in aqueous solution makes it difficult to conduct electrochemical treatment. Even the existence of other alloying elements possesses electrochemical heterogeneity and increases complicacy [13]. Accordingly, corrosion characteristics of AZ31-2WC nanocomposite get deteriorated compared to AZ31 alloy [14]. However, improved corrosion resistance is essential for better durability; the same can be achieved through surface modification and treatment. Consequently, surface treatments of magnesium-based materials are of immense importance for various applications. In this respect, enhancement of surface quality and employment of coating (organic, inorganic, metallic) on magnesium are widely acknowledged [15]. To enhance surface quality, sample surface should be polished properly. Alvarez et al. [16] revealed the importance of surface roughness on corrosion behavior. Walter and Kannan [17] iterated that corrosion tendency of AZ91 alloy enhanced with enhancement in surface roughness.

Among different coating methods, electroless nickel (EN) coating on magnesium is increasingly used to enhance corrosion resistance since a uniform layer can be formed on the material surface without having any curtailment on shape [18]. Literature shows that EN coating can impart a high level of corrosion resistance making it important for electronic industry [19]. Microstructure of coatings can be further modified by applying heat treatment that influences corrosion behavior. Mahallawy et al. [20] have investigated the effect of Ni-P coating on corrosion characteristics of AZ31B, AE42 and ZRE1 magnesium alloys and reported significant improvement in hardness and corrosion resistance. Elsentriecy and Azumi [21] deposited Ni-P coating on AZ91D alloy and examined corrosion characteristics in 3.5% NaCl solution. Experimental results revealed the highest corrosion resistance since the coated sample and coating layer provided complete coverage to the substrate. Wang et al. [22] deposited Ni-P coating on AZ31

alloy using electroless plating technique and annealing was also done on the coated sample. The coated sample possessed higher hardness than the substrate; crystallization further improved hardness value. Electrochemical polarization study revealed the best corrosion resistance for the coated sample followed by crystallized sample and substrate. Abdi-Alghanab et al. [23] developed electroless Ni-P coating on AM60B magnesium alloy considering LDH coating as under-layer and hydrothermal processing was further conducted for different processing time. Corrosion resistance was found to enhance linearly with increase in processing time. Corrosion current density (i_{Corr}) of sample processed for 8 hours was almost 1/7 times of sample processed for 2 hours. Buchtik et al. [24] investigated corrosion behavior of electroless Ni-P coated ZE10 magnesium alloy in 0.1 M NaCl solution. Presence of Ni-P coating resulted in significant improvement in corrosion resistance.

Thus, extensive review of existing literature reveals that incorporation of nanoparticles improves the strength and tribological characteristics while deposition of electroless Ni-P coating may impart higher corrosion resistance. This will essentially yield high strength magnesium-based material having higher corrosion resistance. To the best of authors' knowledge, such studies have not been reported in literature. The present study tries to fill in that gap in the referential literature. In this study, autocatalytic Ni-P coating is deposited on AZ31-2WC nanocomposite to enhance its corrosion resistance. Role of surface roughness, Ni-P coating and heat treatment on corrosion resistance is experimentally evaluated. Corrosion morphology is further studied using scanning electron microscopy.

2. EXPERIMENTAL DETAILS

2.1 Fabrication of nanocomposites

In the present study, AZ31 magnesium alloy is considered as base matrix and 2 wt% of WC nanoparticles (80 nm) are used as reinforcement to produce AZ31-2WC nanocomposite. Compositional details of AZ31 alloy and WC particles are presented in Table 1 and Table 2, respectively. AZ31-2WC nanocomposite is developed in a specially oriented furnace that has resistance heating facility, powder heating set up, mechanical stirrer, ultrasonic vibrator, mold heater, and bottom pouring arrangement (Fig.1). Initially, AZ31 alloy is fed into the crucible of the main furnace and temperature is set at 750°C. Simultaneously, the required amount of WC particulates is heated at 300°C before fortifying in the melt. Pre-heating typically helps to eliminate moisture content, enhance wettability and protect reinforcements from getting burn out. Alloy ingots melt after a definite time. The mechanical stirrer is used inside the melt at a speed of 500 rpm to generate vortex. Pre-heated WC particulates are injected inside that vortex constantly.

Table 1 Chemical conformation of AZ31 alloy

Element	Si	Fe	Zn	Al	Mn	Mg
Wt. %	0.10	0.005	1.20	3.20	0.28	Balance

After completion of particle injection, the stirring speed is escalated to 600 rpm and continued for 5 minutes. Afterwards, the mechanical stirrer is replaced by the ultrasonic horn to provide a high frequency ultrasonic vibration in the mixture. Ultrasonic vibration is continued for 5 minutes. Next, vacuum pouring is done through the bottom pouring hole. Finally, the solidified bar is removed from the split die. Samples are then machined properly to produce desired samples. Fabrication method is minutely discussed elsewhere [9].

Table 2 Features of WC particles

Features	WC nano-powder
Purity	99.9%
Elastic modulus (E)	530-700 GPa
Melting point	2870°C
Color	Black
Particle Size	80 nm

Table 3 Specifications for electroless Ni-P bath

Bath parameters	Details
Nickel sulfate	20 g/l
Nickel chloride	20 g/l
Lead acetate	1 mg/l
Sodium succinate	12 g/l
Sodium hypophosphite	10-20 g/l
Temperature	90 ºC
pH	4.5
Volume of bath	200 ml
Coating duration	2 hours

2.2 Coating deposition

AZ31-2WC nanocomposite samples with size (20×20×8) mm of roughness grade R_a = 0.4 μm are prepared for Ni-P coating deposition. Coating deposition set up is shown as Fig. 2. Primarily, the substrates are rinsed properly to get rid of any foreign particle and corrosion products. Then the samples are air dried followed by pickling treatment in 18% HCl for 1 min and rinsed in deionised water. Initially, a number of trials were performed to finalize composition of bath. Bath decomposition after 15-30 minutes was encountered. Bath decomposition was prevented by adding a limited amount of lead acetate. Details of the bath constituents and the operating parameters are tabulated in Table 3. Acid-pickled and rinsed sample is dipped in palladium chloride solution for 30 sec to activate it and finally dipped in the heated bath (90°C). Palladium chloride helps to achieve good deposition rate from the very beginning. Coating process is continued for 2 hours during which pH of solution is maintained at 4.5. After completion of coating process, samples are taken out of the bath and washed in distilled water. Two different levels of sodium

hypophosphite (10 g/l & 20 g/l) are considered. Some coated samples are also heat treated at 400°C for 1 hour and air-cooled.

Fig. 1 Pictorial view of fabrication unit

Fig. 2 Pictorial view of coating deposition set up

2.3 Characterization

Basic characterization of base alloy, AZ31-2WC nanocomposite and coated samples are performed with the help of SEM (JEOL, Japan & Zeiss) micrographs. Compositional analyses of those samples are carried out using EDX (JSM-6360, Japan) and XRD

analysis (Rigaku, Ultima III). For XRD, Cu Kα source is employed and analysis is performed between scanning ranges of 20°-90° for scanning rate of 2° 2θ/min. Characterization of base alloy and nanocomposite is performed after preparing the sample surfaces. Samples are initially polished with different grit (1500, 2000 & 2500) emery paper. Then those samples are polished on fine clothes using distilled water and polishing agent. Final polished samples are etched in acetic-picral solution (4 g picric acid, 10 ml acetic acid, 70 ml ethanol and 10 ml distilled water). Corroded samples are finally characterized using SEM micrographs.

2.4 Microhardness

Vicker's microhardness of AZ31 alloy, AZ31-2WC nanocomposite, as-coated Ni-P sample and heat-treated sample are studied according to ASTM E384-16 with the help of the UHL microhardness tester (Technische Mikroskopie). A diamond indenter having apex angle 136° is used for this study. As experimental condition, 50 gf load and 10 s dwell time have been fixed. Typically, the average of five readings is taken as microhardness value.

2.5 Surface Roughness Test

Effect of surface roughness (SR) on corrosion behavior is widely acknowledged by scientific community. Accordingly, in this study initial SR of the specimens is assessed with 3D surface profiler (Bruker). Afterwards, a similar sample is smoothened with abrasive paper (400 grit, SiC) and SR is measured with the same instruments. Surface profiler provides 2D as well as 3D surface plots of the tested specimens in attached computerized system.

2.6 Corrosion Study

Corrosion behavior of the developed samples is investigated by performing potentiodynamic polarization test and electrochemical impedance spectroscopy (EIS) using 3.5% NaCl solution in a potentiostat (Gill AC, UK). Contact area of each sample with electrolyte is 1 cm^2. Composite and coated specimens are cleaned properly using acetone and employed as working electrode. The working electrode is attached to the potentiostat at actual position. Saturated calomel electrode is chosen as reference electrode because it comes up with steady potential. Here, platinum electrode is considered as auxiliary electrode as it helps alternate current to find an alternative way in electrolyte. These two electrodes are placed properly in the glass cylinder and working electrode (sample) is clamped properly so that 1 cm^2 area comes in contact with electrolyte solution. Open circuit voltage takes 15 minutes to become steady. The potentiostat coupled with a computerized system helps to explore the corrosion results. For this study, the corrosion potentials at the beginning and end of study are -250 mV and 250 mV whilst the scanning rate is 1 mV/s. EIS results are scrutinized with the pre-installed software with the best fitting semi-circle technique. Corrosion current density (i_{corr}) and potential (E_{corr}) are examined from the Tafel plot by the Tafel extrapolation technique.

3. RESULTS AND DISCUSSION

3.1 Characterization

Basic characterization of the developed materials is performed using SEM micrographs, EDX analysis and XRD analysis. Primarily, SEM micrographs are examined to check the distribution of reinforcement phase in matrix. SEM micrographs of AZ31, AZ31-2WC, as-coated sample and heat-treated sample are presented in Figs. 3a, 3b, 3c & 3d, respectively. In SEM micrographs of AZ31 and AZ31-2WC, α-Mg and β-$Mg_{17}Al_{12}$ are present. SEM micrograph of nanocomposite (Fig. 3b) discloses clear composite structures having finer grain structures. WC particles are almost uniformly dispersed in matrix without having any significant agglomeration. SEM micrograph of as-coated sample surface (Fig. 3c) is optically smooth without having any significant porosity and surface damage. Many globular particles are observed on the surface of as-coated sample. SEM micrograph of heat-treated sample (Fig. 3d) possesses some modifications in both microstructure and crystal structure. After heat treatment, crystal growths of microcrystalline deposits enhance.

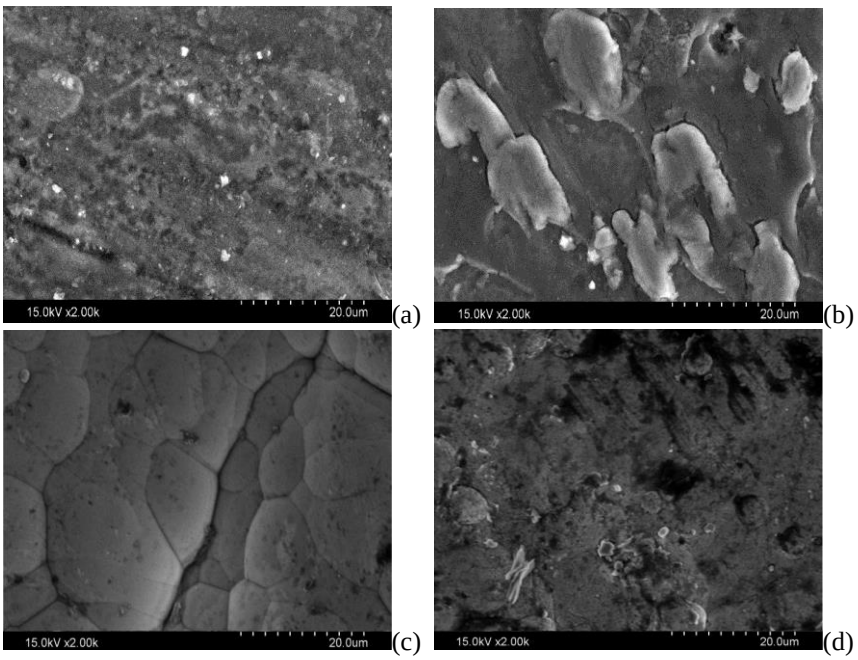

Fig. 3 SEM micrograph (a) AZ31 alloy, (b) AZ31-2WC, (c) Ni-P coating and (d) Heat-treated Ni-P coating

Furthermore, compositional details of samples are scrutinized using EDAX and XRD analysis. EDAX spectrum of AZ31-2WC and as-coated Ni-P coating is shown in Figs. 4a and 4b, respectively. Fig. 4a shows spectrums of Mg, Zn, W, C and O. Basic elements of base alloy are present. Peak of W confirms inclusion of WC particles. However, the exact

percentages of each element are not present as a small area is scanned and particles are of nano-metric scale. EDAX spectrum of as-coated (Fig. 4b) sample shows peak of Ni and P. Basic composition of as-coated sample is determined with regard to wt.% of Ni and P from EDAX spectrum. Weight percentages of Ni and P for as-coated and heat-treated samples are tabulated in Table 4. Amounts of phosphorous in as-coated and heat-treated sample are 9.2% and 11.4%, respectively. Hence, coatings recline in high phosphorous scale. Typically, crystallinity as well as microstructural integrity highly build upon the amount of phosphorous which consequently decides hardness value. From EDAX result amorphous nature of coating can be expected. Phase structures are further revealed by XRD study. XRD results (Fig. 5a) of AZ31-2WC reveals peak of Mg (2θ = 32.16°, 34.58°, 48.14°, 57.17° & 63.54°), WC (36.01° & 48.18°) and W_2C (36.01° & 48.18°). XRD result of heat-treated coating sample is illustrated in Fig. 5b. Fig. 5b possesses peak of Ni, Ni_2P and Ni_3P. This result is in line with phase transformation characteristics of amorphous coating (Ni-P) developed through EN method.

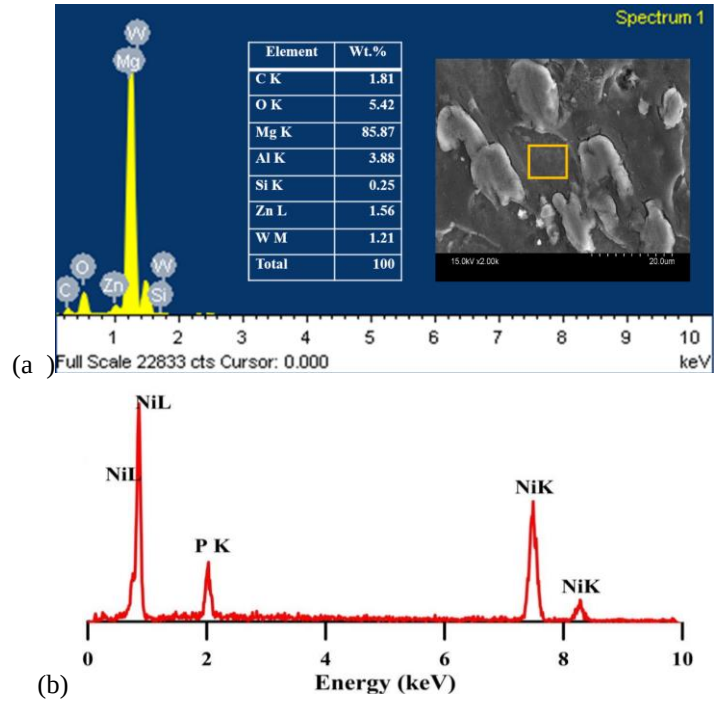

Fig. 4 EDAX spectra (a) AZ31-2WC nanocomposite and (b) Ni-P coated AZ31-2WC sample

Table 4 Wt. % of different elements in coatings

Sample	% of Nickel	% of phosphorous	Total
As-coated	90.8	9.2	100
Heat treated (400°C)	88.6	11.4	100

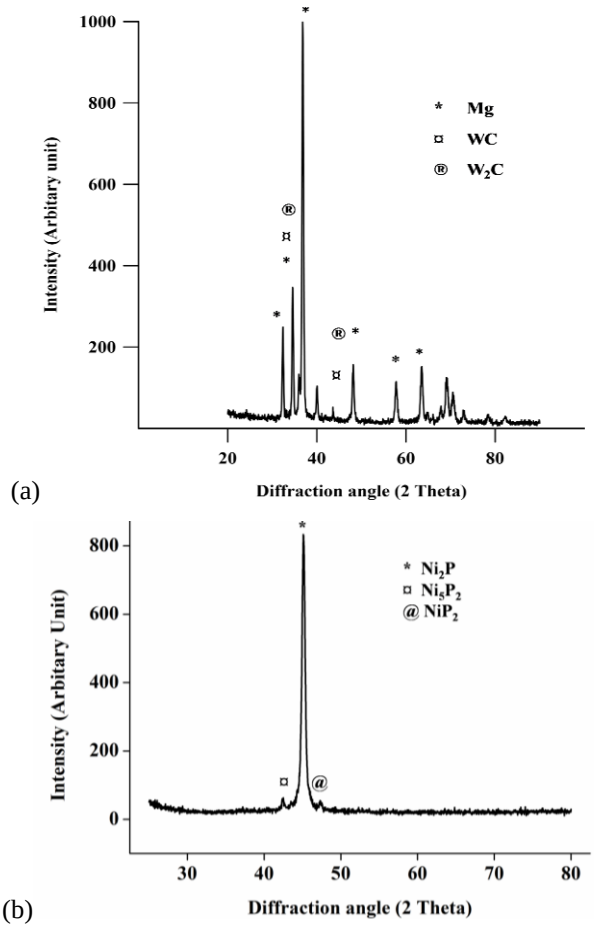

Fig. 5 XRD plot (a) Mg-2WC nanocomposite and (b) Heat-treated coating sample

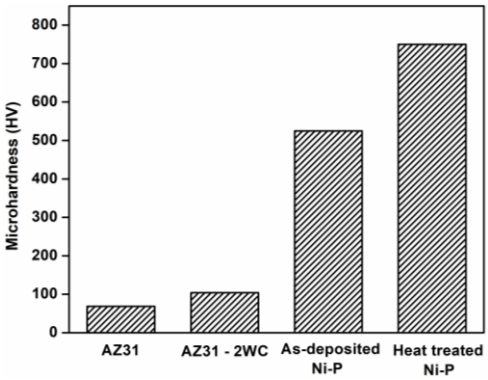

Fig. 6 Microhardness plot: a comparison between base alloy AZ31, nanocomposite AZ31-2WC, as-deposited Ni-P coating and heat treated Ni-P coating

3.2 Microhardness

It is well established in literature that incorporation of reinforcements or deposition of coating enhances microhardness of base alloy. Effects of incorporation of WC particles and deposition of Ni-P coating on microhardness are shown in Fig. 6. It is observed that incorporation of 2wt. % of WC enhances microhardness by 52.45% as compared to AZ31 alloy. As-coated Ni-P (20 g/l) helps to enhance microhardness value significantly. Microhardness value enhances by almost seven times than the base alloy for as-coated Ni-P sample while the heat-treated coating sample possesses around ten times enhancement.

3.3 Corrosion test

Potentiodynamic polarization plots of AZ31, AZ31-2WC and polished sample (AZ31-2WC polished with 400 grit SiC paper) are shown in Fig. 7. Each plot contains anodic section and cathodic section. Study of anodic section is necessary to examine corrosion characteristics as anodic section mainly helps to understand transformation technique of material from sample surface [25]. For clarity, surface roughness profile of polished AZ31-2WC sample is shown in Fig. 8 and surface roughness values of normal sample and polished sample are tabulated in Table 5. Fig. 7 illustrates that corrosion performance initially decreases due to incorporation of 2wt. % of WC but polished sample possesses better corrosion resistance. However, no noticeable differences in cathodic current values are observed. Hence, corrosion characteristics of examined materials are mainly contingent on anodic characteristics. However, clarity can be brought by precisely calculating current density (i_{corr}) and corrosion potential (E_{corr}). Potentiodynamic polarization plots are extrapolated by tafel extrapolation to compute values of E_{corr} and i_{corr} for each curve. Computed values are presented in Table 6. Literature reported that subordinate value of i_{corr} and superior value of E_{corr} imply better corrosion characteristics [26]. Table 6 yields that polished sample possesses better corrosion resistance than base alloy and AZ31-2WC nanocomposite as corrosion potential of polished sample is -1.42V whereas that of AZ31 is -1.43V. This trend is in line with observations reported in literature [16].

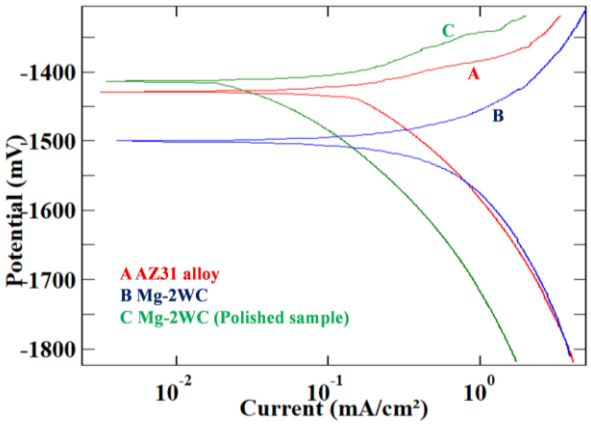

Fig. 7 Potentiodynamic polarization plot for AZ31, AZ31-2WC and polished samples

Table 5 Surface roughness of normal sample & polished sample

Sample	Roughness (R_a), µm
Normal sample	0.916
Polished sample	0.568

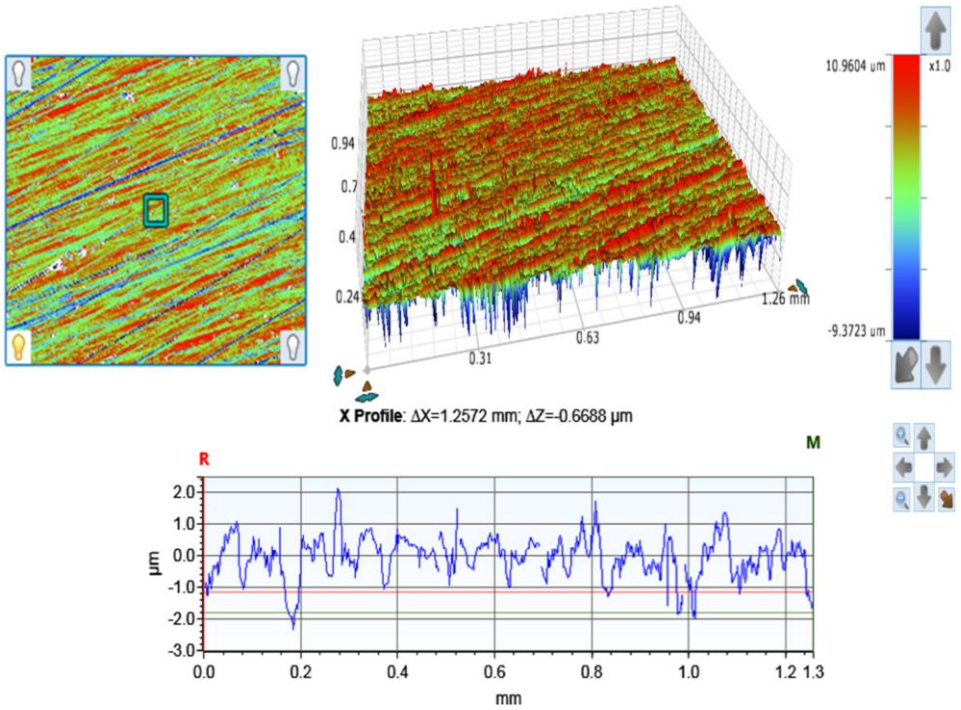

Fig. 8 Surface roughness profile of polished AZ31-2WC sample

Potentiodynamic polarization plot of as-coated Ni-P samples with different $NaH_2PO_2.H_2O$ concentrations (10 g/l & 20 g/l) and corresponding heat-treated samples are presented in Fig. 9. Tafel extrapolation results of these plots are presented in Table 6. It is noticed that i_{corr} value decreases remarkably compared to base alloy and AZ31-2WC sample due to application of Ni-P coating on AZ31-2WC sample. E_{corr} value of as-coated sample also swings toward positive direction compared to substrate sample (AZ31-2WC). Moreover, i_{corr} decreases further and E_{corr} enhances as concentration of $NaH_2PO_2.H_2O$ changes from 10 g/l to 20 g/l. These results iterate that corrosion resistance of AZ31-2WC enhances due to application of Ni-P coating and corrosion resistance enhances further with enhancement in concentration of $NaH_2PO_2.H_2O$. Similar conclusion has been drawn by Diegle et al. [27]. Potentiodynamic polarization curves of heat-treated coated samples are also presented in Fig. 9 and Tafel extrapolation results are presented in Table 6. For heat-treated samples, no specific trend is available as corrosion resistance deteriorates compared to as-coated sample for 10 g/l heat-treated sample while corrosion resistance enhances for 20 g/l heat treated sample compare to as-coated sample. The

highest corrosion resistance is observed for the heat-treated sample having 20g/l sodium hypophosphite. Literature reveals that a higher amount of sodium hypophosphite accompanies to incorporate a higher amount of phosphorous which helps to resist pitting corrosion [28].

Table 6 Tafel extrapolation results

Material	E_{corr} (V)	i_{corr} (mA/cm^2)
AZ31	-1.43	0.0714
AZ31-2WC	-1.50	0.1162
Polished sample	-1.42	0.0687
As-coated (10 g/l)	-0.485	0.0056
Heat-treated (10 g/l)	-0.502	0.0101
As-coated (20 g/l)	-0.394	0.0028
Heat-treated (20 g/l)	-0.377	0.0025

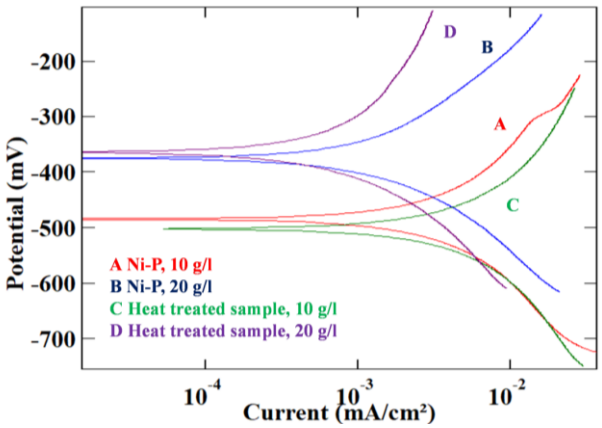

Fig. 9 Potentiodynamic polarization plot of Ni-P coated samples and heat-treated samples

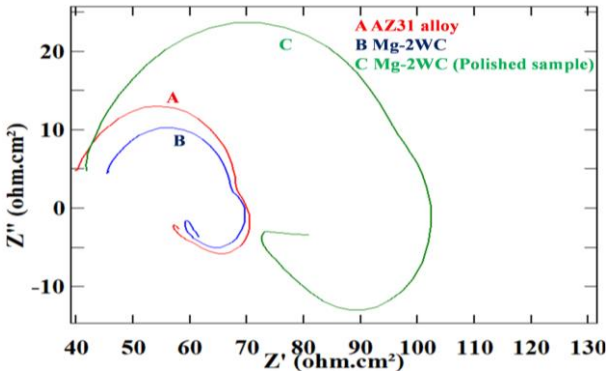

Fig. 10 Nyquist plots of AZ31, AZ31-2WC and polished sample

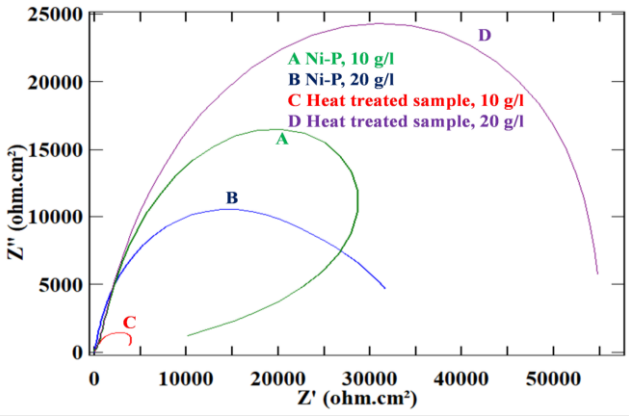

Fig. 11 Nyquist plot of as-coated Ni-P samples heat-treated samples

Corrosion characteristics are further analyzed with the help of Nyquist plot. Nyquist plots of AZ31, AZ31-2WC and polished sample tested at 3.5% NaCl are presented in Fig. 10. Nyquist plots of each sample contain a high frequency capacitive loop, one medium frequency capacitive loop along with a low frequency inductive loop. Typically, rudimentary nature of plots is similar for AZ31, AZ31-2WC and polished samples apart from diameter of plots. This nature is similar to the findings of Wu et al. [29] who reported that polarization resistance is proportional to the diameter of capacitance loop. On the other hand, diameter of capacitance curve is also proportional to corrosion resistance. Thus, it can be concluded from Fig. 10 that sample polished with 400 grit paper is the most corrosion resistive one. Literature also reveals that high frequency capacitive arc relates electrolyte-surface film interface while low frequency capacitive arc signifies diffusion of ion between material and generated film. Low frequency inductive arc indicates localized corrosion due to electrolyte diffusion between film and material [25]. As the polished sample possesses the highest capacitive loop (Fig. 10) among these three samples (AZ31, AZ31-2WC & polished sample), it can be said that there must have more protective layer at film-electrolyte interface, which helps to protect the sample surface from destructive ions.

Nyquist plot of as-coated Ni-P samples with varying sodium hypophosphite and corresponding heat-treated samples are presented in Fig. 11. Here Nyquist plot of all samples possess high frequency capacitive loop having single semicircular shape with varying diameter within frequency range of 10 kHz to 0.01 Hz. Similar shape with variation in diameter of semicircle signifies similar elementary mechanism of corrosion but for different amount of area. Literature reveals that diameter of capacitive loop indicate charge transfer resistance which is directly related to corrosion resistance of that sample. Hence, sample having capacitive loop with highest diameter is the most corrosion resistive one within experimental range. Among as-coated samples, the sample with sodium hypophosphite concentration 20 g/l shows semicircle with the highest diameter. Hence, that sample has the highest corrosion resistance. It is obvious from Fig. 11 that samples possess charge transfer controlled behavior in electrolyte solution. However, as-coated sample having sodium hypophosphite concentration 10 g/l possesses proneness of

starting another semicircle. Probable reason of such nature is piercing by electrolyte and forming local electrochemical cell which deteriorates corrosion resistance. Similar observation is noted by Zhang et al. [30]. Obtained curves are analyzed to obtain values of R_{ct} and C_{dl}. Among tested samples, as-coated sample with sodium hypophosphite concentration 20 g/l shows the highest R_{ct} value (34 kohm.cm^2) and the lowest C_{dl} value (26 μF). R_{ct} value and C_{dl} value of as-coated sample with sodium hypophosphite concentration 10 g/l is 14.7 kohm.cm^2 and 41 μF, respectively. Literature revealed that corrosion characteristics of Ni-P coating mainly rely on amorphous nature of coating and amount of phosphorous. Ni-P coating having high phosphorous content results higher corrosion resistance because of more amorphous and homogeneous structure. Structural homogeneity and higher phosphorous content reduce porosity of coating. Reduced porosity also protects sample surface from infiltration of corrosive parameters. These findings are in line with literature [30]. Nyquist plot of heat-treated coated samples are also presented in Fig. 11. It is observed that the largest semicircle is present for heat-treated coating sample with 20 g/l sodium hypophosphite. Hence, this sample is the most corrosion resistive one among all tested samples. EIS results are following same trend of previously discussed tafel plot. Among heat-treated samples, sample with sodium hypophosphite concentration 20 g/l shows the highest R_{ct} value (59.5 kohm.cm^2) and the lowest C_{dl} value (21.9 μF). Hence, this is the most corrosion resistive sample among heat-treated sample. Literature reveals that Ni-P coating become denser as well as less porous after heat treatment. Heat treatment also generates secondary phase like Ni_aP_b which protects the sample surface from corrosion [31]. Similar phenomenon may have occurred for the present study.

3.4 Corrosion morphology

Corrosion characteristics of the developed materials are further analyzed using SEM images of corroded surfaces. SEM micrograph of corroded surface helps to understand typical corrosion mechanism which occurred during experimentation. SEM images of corroded surfaces of AZ31, AZ31-WC nanocomposite and polished sample are presented in Fig. 12. SEM micrographs of corroded zones of these three specimens are filled with volcano-like sediments which are mainly insoluble corrosion by-products. Cracks of different shapes and sizes are also present in corroded surfaces. Similar nature is also mentioned by Ascencio et al. [32] in their study. Literature also illustrated that cracks are usually formed because of dehydration of deposited layers [33]. Destructive electrolytes (Cl^-) of NaCl solution infiltrate through those cracks and touch material surface. As a result, corrosion rate increases [17]. Hence, illustration of position, nature and intensity of crack is necessary to predict corrosion characteristics of AZ31, AZ31-2WC nanocomposite and polished sample. SEM micrographs (Fig. 12) clearly show that the corroded surface of the polished sample (Fig. 12c) contains lesser amount and intensity cracks than the corroded surfaces AZ31 (Fig. 12a) and AZ31-2WC (Fig. 12b). On the other hand, the corroded surface of AZ31 possesses lesser intensity cracks than the corroded surface of AZ31-2WC. Hence, the intensity of cracks lies in order of AZ31-2WC > AZ31 > polished sample. So, the chances of penetration of Cl^- ions are greater for AZ31-2WC followed by AZ31 and polished sample. Thus, corrosion resistance should lie

in order of polished sample > AZ31 > AZ31-2WC. Similar trend is observed in Tafel plot and Nyquist plot.

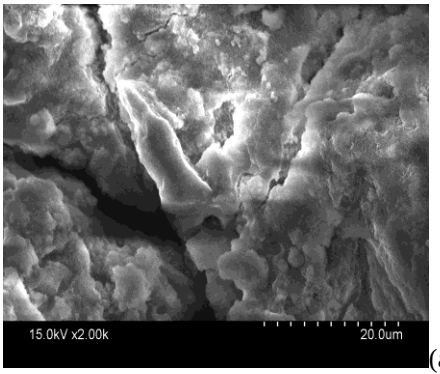

(a)
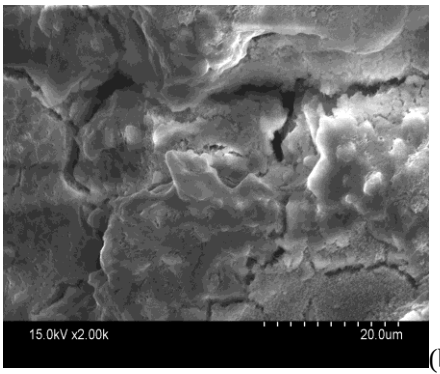

(b)
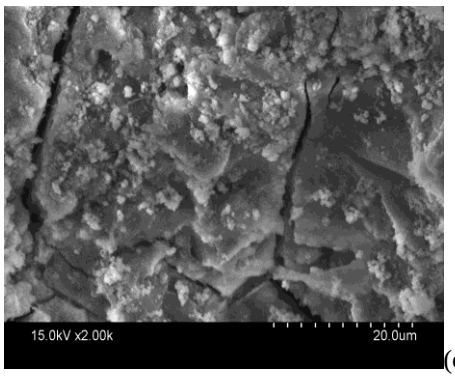

(c)

Fig. 12 SEM micrographs of corroded surface (a) AZ31, (b) AZ31-2WC and (c) Polished sample

SEM images of as-coated and heat-treated (HT) samples are presented in Fig. 13. SEM images of as-coated and HT samples almost possess similar morphology; that is why coating having the highest corrosion resistance (Sodium hypophosphite-20 g/l) is discussed here for brevity. Very fine pores are present in the corroded surface of both as-coated and heat-treated samples. These pores make route for electrolyte solution to reach the sample surface. Thus, galvanic cells are formed between Ni-P coat and substrate surface. Fig. 13 also shows that the pores in heat-treated samples are scanty compared to as-coated sample. That is why the heat-treated sample exhibits a much lesser deleterious effect compared to as-coated sample. Even the less porous nature of the heat-treated sample intercepts the propagation of harmful effect below the coating and protects the substrate surface. However, SEM images of both as-coated and HT samples do not possess cracks like substrates surface. Thus, as-coated and HT samples must result in superior corrosion resistance compared to base alloy, nanocomposite sample and polished sample, which is already shown by Tafel plot and Nyquist plot. Similar results are reported by El Mahallawy et al. [20].

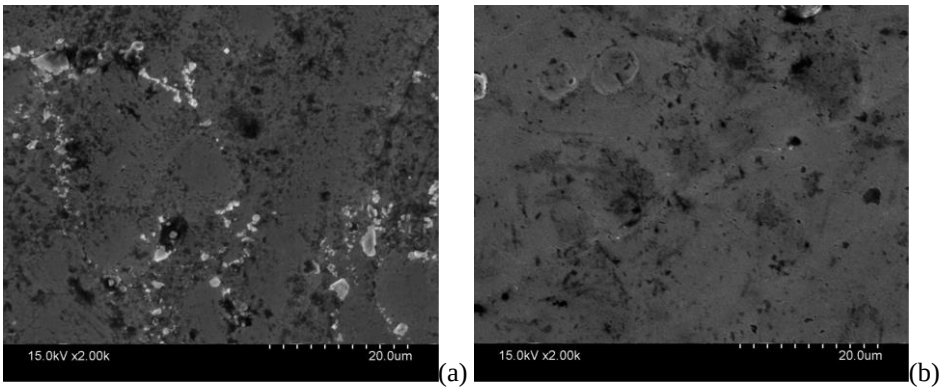

(a) (b)

Fig. 13 Corroded surface (a) As-coated sample (Sodium hypophosphite-20 g/l) and (b) Heat-treated sample

Over the years, EN coating has emerged as a widely acknowledged method for surface modification [34]. Nevertheless, the conventional coating methods (electro-deposition & electroless plating) suffer from environmental issues due to disposal of toxic elements [35]. As a result, the concepts of cleaner production using chemical vapor deposition (CVD) and physical vapor deposition (PVD) are coming up [36]. However, EN coating cannot be overlooked as it possesses some useful advantages like mass production capability, coating ability on any substrate and shape. Accordingly, incorporation of the concept cleaner production in electroless coating (making the bath more eco-friendly) is gradually drawing attention of researchers [37].

4. CONCLUSION

In the present study, the result of fortification of WC nanoparticles in AZ31 alloy, surface roughness, Ni-P coating and its heat-treatment on corrosion behavior is examined using 3.5% NaCl solution. AZ31-2WC nanocomposites are produced using ultrasonic vibration supported stir casting technique. Electroless Ni-P coatings with different concentration of sodium hypophosphite (10 g/l & 20 g/l) are deposited on AZ31-2WC nanocomposite and the coated sample is further heat-treated. Conclusions from the present study are listed below:

- SEM micrograph of nanocomposite reveals that the composite has finer grain structures. SEM micrograph of as-coated sample surface is optically smooth without having any significant porosity and surface damage. Many globular particles are observed on the surface of as-coated sample. EDAX analysis confirms inclusion of WC particles. Basic composition of as-coated sample is determined with regard to wt. % of Ni and P from EDAX spectrum. Amounts of phosphorous in as-coated and heat-treated sample are 9.2% and 11.4%, respectively. XRD result of heat-treated coating sample illustrated peak of Ni, Ni_2P and Ni_3P.
- Incorporation of 2wt. % of WC enhances microhardness by 52.45% compared to base alloy. Microhardness value enhances by almost seven times for as-coated Ni-P

compared to base alloy while heat-treated coating sample possesses around 10 times enhancement.

• Potentiodynamic tests and EIS study are carried out using 3.5% NaCl solution for all samples. Among AZ31, AZ31-2WC and polished sample, polished sample possesses better corrosion resistance than base alloy and AZ31-2WC nanocomposite. Corrosion resistance of AZ31-2WC enhances due to deposition of Ni-P coating; it enhances further with higher concentration of NaH_2PO_2. H_2O (20 g/l) in electroless bath. Heat-treated coating sample with 20 g/l sodium hypophosphite is the most corrosion resistive one among all tested samples. Very fine pores are present in corroded surface of both as-coated and heat-treated samples. These pores make route for electrolyte solution to reach the sample surface. Pores in heat-treated samples are scanty compared to as-coated sample. That is why heat-treated sample exhibit a lesser deleterious effect compared to as-coated sample.

REFERENCES

1. Kulekci, M.K., 2008, *Magnesium and its alloys applications in automotive industry*, The International Journal of Advanced Manufacturing Technology, 39(9-10), pp. 851-865.
2. Avedesian, M.M., Baker, H. eds., 1999, *ASM specialty handbook: magnesium and magnesium alloys*, ASM international, 274 p.
3. Casati, R., Vedani, M., 2014, *Metal matrix composites reinforced by nano-particles—a review*, Metals, 4(1), pp. 65-83.
4. Nguyen, Q.B., Sim, Y.H.M., Gupta, M., Lim, C.Y.H., 2015, *Tribology characteristics of magnesium alloy AZ31B and its composite*, Tribology International, 82, pp. 464-471.
5. Erman, A., Groza, J., Li, X., Choi, H., Cao, G., 2012, *Nanoparticle effects in cast Mg-1 wt% SiC nano-composites*, Materials Science and Engineering: A, 558, pp. 39-43.
6. Meenashisundaram, G.K., Gupta, M., 2014, *Low volume fraction nano-titanium particulates for improving the mechanical response of pure magnesium*, Journal of Alloys and Compounds, 593, pp. 176-183.
7. Selvam, B., Marimuthu, P., Narayanasamy, R., Anandakrishnan, V., Tun, K.S., Gupta, M., Kamaraj, M., 2014, *Dry Sliding wear behaviour of zinc oxide reinforced magnesium matrix nano-composites*, Materials & Design, 58, pp. 475-481.
8. Rashad, M., Pan, F., Hu, H., Asif, M., Hussain, S., She, J., 2015, *Enhanced tensile properties of magnesium composites reinforced with graphene nanoplatelets*, Materials Science and Engineering: A, 630, pp. 36-44.
9. Banerjee, S., Poria, S., Sutradhar, G., Sahoo, P., 2019, *Dry sliding tribological behavior of AZ31-WC nano-composites*, Journal of Magnesium and Alloys, 7(2), pp. 315-327.
10. Banerjee, S., Poria, S., Sutradhar, G., Sahoo, P., 2019, *Tribological behavior of Mg-WC nano-composites at elevated temperature*, Materials Research Express, 6(8), 0865c6.
11. Banerjee, S., Poria, S., Sutradhar, G., Sahoo, P., 2020, *Abrasive wear behavior of WC nanoparticle reinforced magnesium metal matrix composites*, Surface Topography: Metrology and Properties, 8(2), 025001.
12. Banerjee, S., Poria, S., Sutradhar, G., Sahoo, P., 2019, *Nanoindentation and scratch resistance characteristics of AZ31–WC nanocomposites*, Journal of Molecular and Engineering Materials, 7(03n04), 1950007.
13. Sharma, A.K., Suresh, M.R., Bhojraj, H., Narayanamurthy, H., Sahu, S.P., 1998, *ISRO Satellite Centre, Bangalore, India*, Metal Finishing, March, pp. 10-18.
14. Banerjee, S., Poria, S., Sutradhar, G., Sahoo, P., 2019, *Corrosion behavior of AZ31-WC nano-composites*, Journal of Magnesium and Alloys, 7(4), pp. 681-695.
15. Gray, J., Luan, B., 2002, *Protective coatings on magnesium and its alloys—a critical review*, Journal of Alloys and Compounds, 336(1-2), pp. 88-113.

16. Alvarez, R.B., Martin, H.J., Horstemeyer, M.F., Chandler, M.Q., Williams, N., Wang, P.T., Ruiz, A., 2010, *Corrosion relationships as a function of time and surface roughness on a structural AE44 magnesium alloy*, Corrosion Science, 52(5), pp. 1635-1648.
17. Walter, R., Kannan, M.B., 2011, *Influence of surface roughness on the corrosion behaviour of magnesium alloy*, Materials & Design, 32(4), pp. 2350-2354.
18. Younan, M.M., Shoeib, M., El-Enin, S.A., 2001, *Plating-Aufsatze-effect of fluoborate anion on electroless nickel-phosphorus alloy deposition*, Galvanotechnik, 92(6), pp. 1531-1540.
19. Singh Raman, R.K., Birbilis, N., Efthimiadis, J., 2004, *Corrosion of Mg Alloy AZ91–the role of microstructure*, Corrosion Engineering Science and Technology, 39(4), pp. 346-350.
20. El Mahallawy, N., Bakkar, A., Shoeib, M., Palkowski, H., Neubert, V., 2008, *Electroless Ni–P coating of different magnesium alloys*, Surface and Coatings Technology, 202(21), pp. 5151-5157.
21. Elsentriecy, H.H., Azumi, K., 2008, *Electroless Ni–P Deposition on AZ91D magnesium alloy prepared by molybdate chemical conversion coatings*, Journal of the Electrochemical Society, 156(2), D70.
22. Wang, C.M., Wang, J.Q., Zhang, B., Niu, R.B., Yu, J.K., Jing, Q., 2013, *Ni–P coating on AZ31 magnesium alloy and its crystallization*, Rare Metals, 32(5), pp. 465-468.
23. Abdi-Alghanab, K., Seifzadeh, D., Rajabalizadeh, Z., Habibi-Yangjeh, A., 2020, *High corrosion protection performance of the LDH/Ni-P composite coating on AM60B magnesium alloy*, Surface and Coatings Technology, 397, 125979.
24. Buchtík, M., Kosár, P., Wasserbauer, J., Tkacz, J., Doležal, P., 2018, *Characterization of electroless Ni–P coating prepared on a wrought ZE10 magnesium alloy*, Coatings, 8(3), 96.
25. Srinivasan, A., Shin, K.S., Rajendran, N., 2014. *Dynamic electrochemical impedance spectroscopy (DEIS) studies of AZ31 magnesium alloy in simulated body fluid solution*, RSC Advances, 4(53), pp. 27791-27795.
26. Rashad, M., Pan, F., Asif, M., Chen, X., 2017, *Corrosion behavior of magnesium-graphene composites in sodium chloride solutions*, Journal of Magnesium and Alloys, 5(3), pp. 271-276.
27. Diegle, R.B., Sorensen, N.R., Clayton, C.R., Helfand, M.A., Yu, Y.C., 1988, *An XPS investigation into the passivity of an amorphous Ni - 20P alloy*, Journal of the Electrochemical Society, 135(5), pp. 1085-1092.
28. Sun, R., Yu, G., Xie, Z., Hu, B., Zhang, J., He, X., Zhang, X., 2015, *Influence of hypophosphite on efficiency and coating qualities of electroless Ni-P deposits on magnesium alloy AZ91D*, International Journal Electrochemical Science, 10, pp. 7893-7904.
29. Wu, L., Wang, C., Pokharel, D.B., Etim, I.I.N., Zhao, L., Dong, J., Ke, W., Chen, N., 2018, *Effect of applied potential on the microstructure, composition and corrosion resistance evolution of fluoride conversion film on AZ31 magnesium alloy*, Journal of Materials Science & Technology, 34(11), pp. 2084-2090.
30. Zhang, S., Cao, F., Chang, L., Zheng, J., Zhang, Z., Zhang, J., Cao, C., 2011, *Electrodeposition of high corrosion resistance Cu/Ni–P coating on AZ91D magnesium alloy*, Applied Surface Science, 257(21), pp. 9213-9220.
31. Rabizadeh, T., Allahkaram, S.R., Zarebidaki, A., 2010, *An investigation on effects of heat treatment on corrosion properties of Ni–P electroless nano-coatings*, Materials & Design, 31(7), pp. 3174-3179.
32. Ascencio, M., Pekguleryuz, M., Omanovic, S.J.C.S., 2014, *An investigation of the corrosion mechanisms of WE43 Mg alloy in a modified simulated body fluid solution: the influence of immersion time*, Corrosion Science, 87, pp. 489-503.
33. Bakhsheshi-Rad, H.R., Hamzah, E., Tok, H.Y., Kasiri-Asgarani, M., Jabbarzare, S., Medraj, M., 2017, *Microstructure, in vitro corrosion behavior and cytotoxicity of biodegradable Mg-Ca-Zn and Mg-Ca-Zn-Bi alloys*, Journal of Materials Engineering and Performance, 26(2), pp. 653-666.
34. Sahoo, P., Das, S.K., 2011, *Tribology of electroless nickel coatings-a review*, Materials & Design, 32(4), pp. 1760-1775.
35. Gomez da Silva, F.J., Gouveia, R.M., 2020, *Practices on cleaner production and sustainability. In: Cleaner production: toward a better future*. Cham: Springer International Publishing, pp. 247-280.
36. Navinšek, B., Panjan, P., Milošev, I., 1999, *PVD coatings as an environmentally clean alternative to electroplating and electroless processes*, Surface and Coatings Technology, 116, pp. 476-487.
37. Bonin, L., Vitry, V., Delaunois, F., 2020, *Replacement of lead stabilizer in electroless nickel-boron baths: synthesis and characterization of coatings from bismuth stabilized bath*, Sustainable Materials and Technologies, 23, e00130.